HORIBA Scientific

AFM-Raman

AFM-TERS measurements in a liquid environment with side illumination/collection

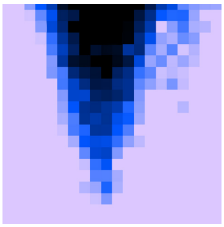

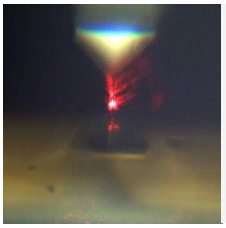

Technical Note

Nanotechnology AFM18

Patrick Hsia[1], Pierre Burgos[2], Alexander Yagovkin[1], Alexey Belyaev[1] & Marc Chaigneau[1]
[1]HORIBA FRANCE SAS, Palaiseau, France. [2]HORIBA UK Ltd., Northampton, UK.

Abstract: The new breakthrough in Raman nanoscale chemical imaging is the measurement in a liquid environment. TERS measurements in liquids have significantly broadened their potential applications across scientific disciplines such as heterogeneous catalysis, electrochemistry, cellular biology and biomaterials. Implementation of TERS in liquids brings out some instrumental difficulties. AFM-TERS in liquids have been published very recently but only in bottom and top optical accesses. In this technical note, the special instrumental features of the TERS setup and experimental conditions of the measurements enabling TERS in liquids using side illumination/collection in order to keep optimal polarization conditions are presented: (i) the design of a side access liquid cell that allows high-throughput optics, (ii) the option to perform AFM imaging in true non-contact mode in liquids, and (iii) the alignment procedure of the Raman laser on the AFM-TERS tip in liquids using an objective mounted on a piezoelectric scanner. These latest instrumental developments are applied to nanoscale imaging of graphene oxide flakes and carbon nanotubes immersed in water. TERS resolution in liquids down to 20 nm is demonstrated along with true non-contact AFM images.

Keywords: AFM-Raman, Tip-Enhanced Raman Spectroscopy (TERS), TERS in liquids, AFM non-contact in liquids.

Introduction

Atomic Force Microscopy (AFM) associated to Raman spectroscopy has proven to be a powerful technique for probing chemical properties at the nanoscale. The AFM tip acts as a nanoantenna that enhances the incident electromagnetic field in a very confined way. As a result, a localized enhanced optical signal can be obtained at the apex of the tip thanks to a complex mix of resonant and non-resonant effects. Techniques like Tip-Enhanced Raman Spectroscopy (TERS) or Tip-Enhanced Photoluminescence (TEPL) can then be associated to the different physical information accessible with the AFM [1]. Nevertheless, some applications require a liquid environment such as in-situ investigation of biological samples, catalysis and electrochemical reactions. The development of AFM-Raman in liquids, with side illumination/collection in order to keep optimal polarization conditions, would open the path to these new perspectives and therefore broaden the applications of TERS.

The first experimental demonstration of TERS in a liquid was performed on a self-assembled monolayer (SAM) with a bottom illumination and collection configuration in 2009 [2]. Bottom backscattered configuration was also used in other works, e.g. for lipid bilayers [3], for catalytic reactions [4], SWCNTs [5], or probing molecules grafted on gold nanoplatelets [6, 7]. While excitation/collection can be performed with high numerical aperture objective in bottom configuration, it is limited to transparent samples and incident polarization may have to be shaped. Top configuration has been used in electrochemistry unraveling mechanisms at the molecular scale [8, 9] and a resolution down to 8 nm has been demonstrated in STM-TERS [10] (Scanning Tunneling Microscopy combined with TERS). Side illumination through a glass window is also well spread in groups like Van Duyne's [11], Ren's [12, 13] or Domke's [14], but all these examples are STM-based and limited to conductive samples.

In this work, a dedicated cell suitable for side optical illumination and collection has been designed to perform AFM-based Tip-Enhanced spectroscopy in a water environment.

Experimental setup

1) Description of the AFM-Raman system, the cell and the optical adaptations:

Correlated AFM-TERS has been performed on graphene oxide (GO) and carbon nanotubes (CNTs) deposited on a gold-coated substrate. The sample has then been immerged in water inside a cell adapted on the sample stage of the OmegaScope AFM (HORIBA France). The 633 nm *p*-polarised laser and Raman signal are brought from and to

a long focal spectrometer (LabRAM HR Evolution, 800 mm focal length, HORIBA France) via an optical coupling (Fig. 1). To collect all Raman peaks of interest in one spectral window, a 300 grooves/mm grating is used.

Figure 1: HORIBA AFM-Raman LabRAM Nano.

The cell is equipped with a glass window for side illumination/collection. Due to the difference of refractive index between air/glass and glass/water, the optical path is corrected using an additional lens placed in front of the side objective. As the cantilever is also in contact with water, the path of the AFM feedback laser diode (1310 nm) is deviated by the change of refractive index between air and water. An additional lens mounted on the cantilever holder itself is also added to correct the diode refraction in water (Fig. 2).

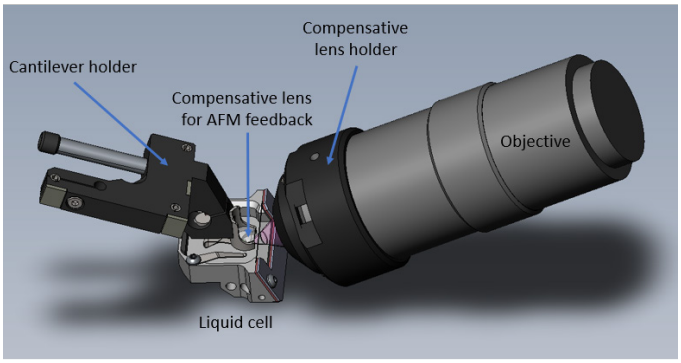

Figure 2: Representation of the liquid cell, the AFM tip holder, the objective, and the optical path (in pink) through the glass window of the liquid cell.

An objective tilted by 30° with respect to the sample plane with a super long working distance is used (Mitutoyo 50×, NA = 0.42, WD = 20.5mm). Although the issue of tip degradation can be addressed [2, 4], the TERS experiments in liquids are performed with gold coated AFM-TERS tips (OMNI-TERS-SNC-Au, AppNano, USA) which are known to have a better stability than silver tips.

2) AFM feedback in water

As described in the first section, the AFM tip holder dedicated to measurements in liquids is equipped with a non-removable lens for the feedback diode of the AFM. A droplet of water is first deposited between the lens and the cantilever in order to make the first AFM adjustments (i.e. the automated tip feedback laser adjustment on the cantilever and centering of the reflection on the four-quadrant photodiode). These adjustments are done before dipping the tip holder into the cell itself.

It is important to stress that the images shown in the results section are acquired in non-contact mode. The oscillation of the cantilever inside water generates several peaks and is highly dampened; for that reason, AFM imaging in contact mode is traditionally used in a liquid environment. The use of non-contact mode imaging in liquids in our experimental setup is made possible by increasing the driving amplitude of the oscillation which helps preserve the tip and the sample from degradation and contamination that can easily happen in contact mode.

3) Tip visualization: towards a coarse alignment of the excitation laser

The OmegaScope AFM optical platform is equipped with two video units enabling the simultaneous visualization of the tip from both top and side optical paths. The optics and AFM tip are fixed while the sample and the cell approach the tip. In this configuration of TERS in liquids, the optical path goes through different diopters, then the focus of the tip observed by the side camera can change when the cell is moved away from or towards the objective during sample retraction/approach. To always keep the tip in focus, and thus simplify the Raman laser-to-tip alignment, the motorized and automated approach of the cell is inclined by 25° (Fig. 3).

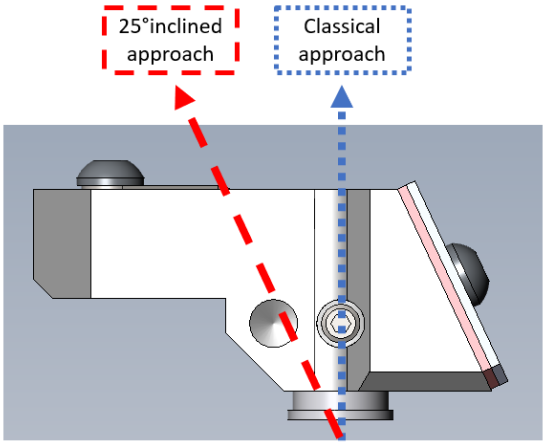

Figure 3 : Side view or the cell. The cantilever (not shown) is positioned above.

As a result, when the approach is completed, the excitation laser can be visible on the tip's apex and its position is already close to the optimal position for TERS measurements in a liquid (Fig. 4). The shape of the laser spot in water is distorted comparing to the one in air, and optical aberrations and parasitic reflections can be observed. Thus, a fine and precise optical alignment is needed to achieve TERS conditions.

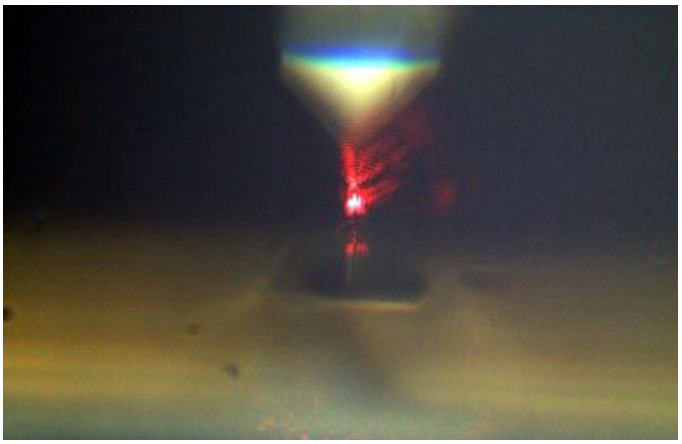

Figure 4: Laser focused in water near the tip apex, viewed by the side camera.

4) Fine optical alignment with the objective scanner

For TERS measurements, the alignment of the excitation laser and the tip is crucial to get the localized enhancement effect at the tip apex. The instrumentation should provide tools to finely focus the laser at the end of the AFM-TERS tip. In our AFM-Raman setup, the tip remains fixed and the excitation laser is brought to the tip's apex thanks to a so-called objective scanner that moves the laser position in a plane but also in depth for focalization. Different mappings with the objective scanner can be done: a scan in a plane at fixed focus (called "XY objective") or in a plan orthogonal to the first one that sweeps the focus (called "XZ objective" or "YZ objective").

XY objective scans are needed to precisely bring the spectroscopic laser spot to the tip apex with an accuracy below 500 nm. Fig. 5a shows objective scanner maps (with an inverted contrast as comparing to TERS in air environment) from the area under the background curve over the whole spectral range (peak area filtering) on a color scale (Fig. 5c). The observed contrast can be attributed to the fact that water diffuses light more significantly than the cantilever/tip. In this case, tip is in the water of the cell but far from the sample. The shape of the tip can be reconstructed. Each pixel contains a background spectrum.

When approached and landed, the XY objective map shows new features. The TERS signal is found at the center of the 'hourglass' (Fig. 5b).

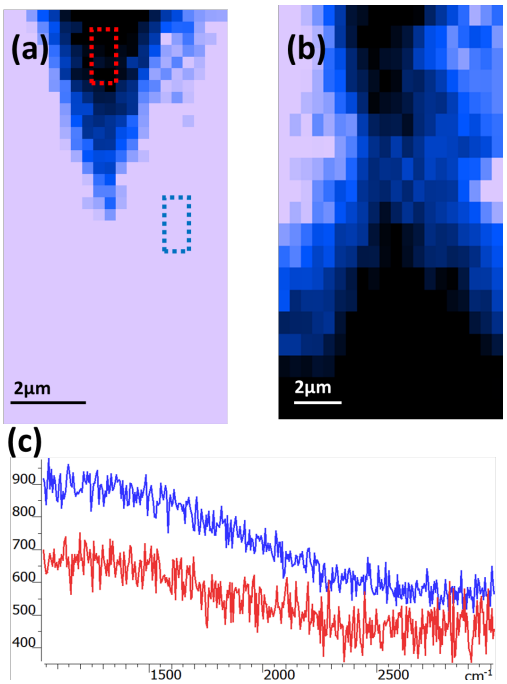

Figure 5: (a) XY objective scan obtained when the tip is few millimeters from the sample's surface, (b) XY objective scan after the approach when the tip is interaction with the sample's surface, (c) background spectra from the selected colored rectangles in Fig. 5a.

Results

1) Non-contact AFM images in liquid environments

AFM images of graphene oxide (GO) flakes and CNTs were recorded in true non-contact mode with Au coated AFM-TERS tips (Fig. 6).

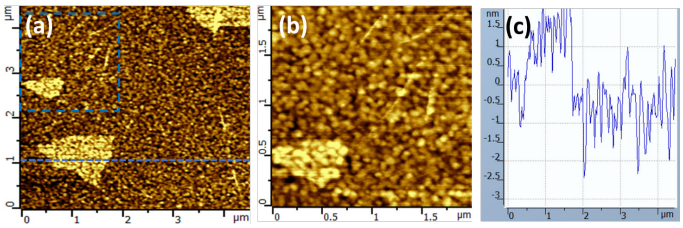

Figure 6: (a), (b) AFM topographic images of the sample in water obtained in true non-contact mode (256 × 256 pixels), (c) section analysis of the topographic signal along the dotted blue line on the AFM map.

Graphene oxide flakes along with carbon nanotubes are clearly discernable despite the roughness of the gold substrate. Mean roughness and RMS roughness are both inferior to 1 nm (averaging on the substrate shows RMS roughness of 700 pm, and 750 pm RMS roughness on the graphene flake) which clearly indicates high sensitivity in

terms of AFM measurements. The section analysis of the topographic signal presented in Fig. 6c shows a 840 pm step of graphene oxide. The image quality in non-contact mode is well preserved in water environment.

2) TERS mapping on GO and CNTs and calculation of the enhancement factor EF.

A TERS map in water of GO flakes and CNTs (2.2 × 1 µm (75 × 22 pixels)) is collected with a 2 s integration time spectrum at each pixel (30 nm step). The full TERS map is recorded in 1h and 50 minutes and illustrates the great stability of both the AFM system and the optical coupling (Fig. 7).

Both topographic images and TERS maps are collected at the same time using a special mode called "Spec-Top™" [15] mode with "dual spec" option: for each pixel (i) one spectrum (sum of the near-field and far-field signals) is acquired with tip in direct contact with the surface with a typical interaction force of 2-10 nN and (ii) another spectrum is acquired with tip in tapping mode (a few nm away from the sample surface, considered to be the far-field contribution (FF)). In between two pixels of the map, the sample moves in semi-contact mode to preserve the sharpness and plasmonic enhancement of the tip.

GO and CNTs are both graphitic materials sharing similarities in their Raman spectra. Around 1600 cm^{-1} is located a G band that represents in-plane tangential movement of the carbon atoms and occurs in any graphite related material. Another around 1350 cm^{-1}, the D band ("D" stands for defects) is seen in both GO and CNTs. This vibration is visible only if defects are present in the carbon lattice. As a result, this band is used as an indication of the sample defect density. In otherwise structurally pristine carbon materials, a band around 2650 cm^{-1} is present: 2D band (sometimes called G'). This band is not to be found with GO as its sp^2 structure is very disturbed by the adjacent functional groups. Additionally, GO can be distinguished from CNTs by the broader D and G [16, 17] bands.

In the TERS map plotting the D band intensity (Fig. 7c) both GO and CNTs are visible. Higher concentration of defects is observed in the CNTs themselves and in GO oxide wrinkles and edge [18]. The TERS map plotting the 2D band intensity (Fig. 7b) shows only the contribution of the carbon nanotubes. Thus, the two species can be clearly distinguished from each other. Their different Raman signatures are shown in the TER spectra plotted in Fig. 7d.

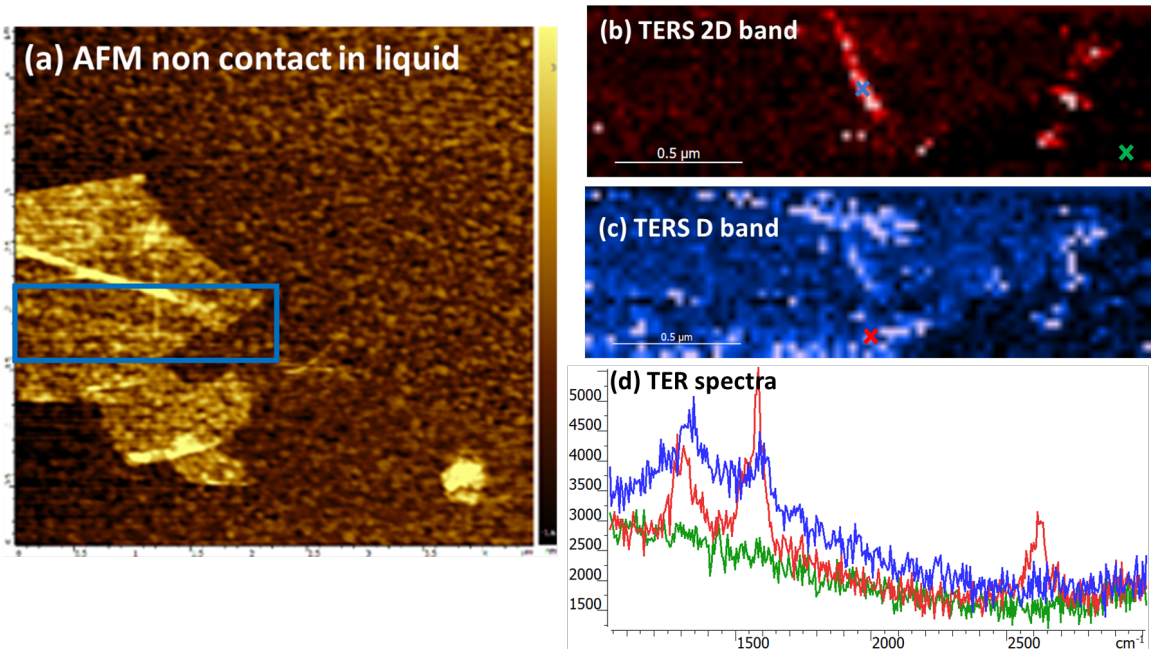

Figure 7: (a) AFM imaging (true non-contact mode) of graphene oxide flake in water, (b) TERS map of the 2D band and (c) TERS map of the D band, (d) typical TER spectra taken from the cross points on the TERS images.

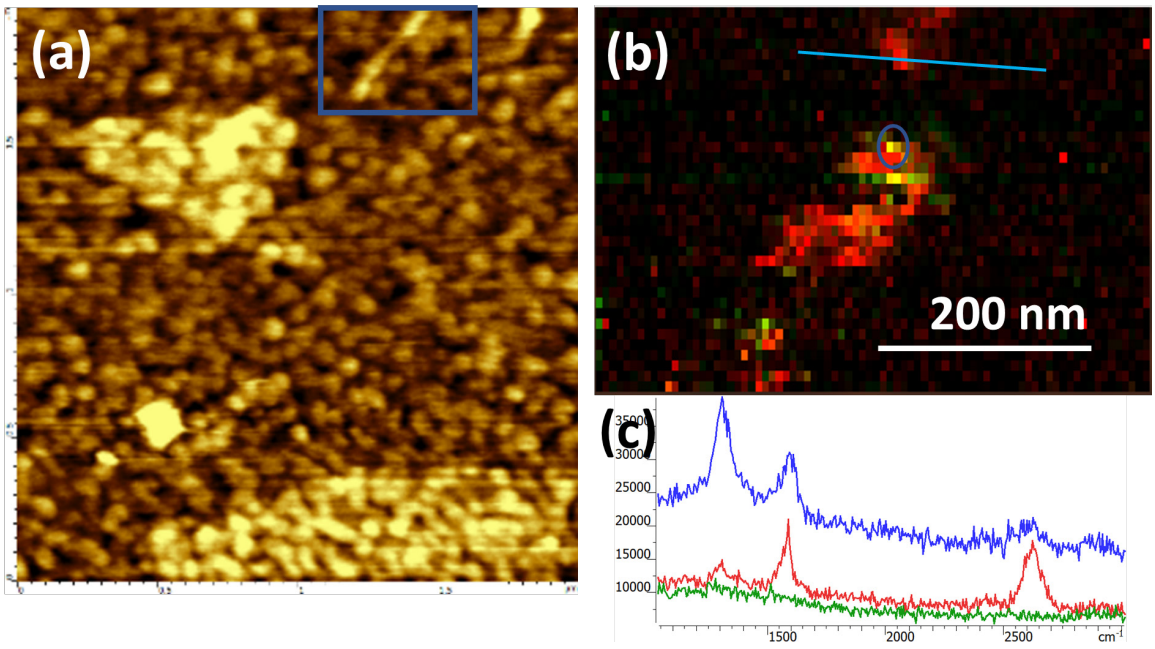

Figure 8: Correlated AFM-TERS measurements on a CNT in water; (a) 2 × 2 µm non-contact AFM image, (b) hyperspectral TERS image in water (overlay of the D and 2D bands intensities), (c) TER spectra in the area indicated by the blue circle. The three Raman spectra are separated by 1.7 nm (adjacent pixels in both X and Y directions).

In order to push the limit of the optical resolution through TERS in liquids, Fig. 8 presents a high resolution TERS image in a liquid of an individual CNT, 500 × 350 nm scanning area (300 × 200 pixels)), 2 s integration time spectrum at each pixel (1.7 nm step). The pure far-field map shows a homogeneous background with no Raman signature (not shown), whereas the near-field + far-field map shows peaks related to a single CNT (Fig. 8 b). The TERS map (Fig. 8 b in which D band is shown in yellow and 2D band in red) also demonstrates a chemical sensitivity down to the pixel size (1.7 nm): e.g. the intensity of the D peak at ~1350 cm^{-1} in the blue circle marked area close to the local lattice defects rises drastically from one pixel to the adjacent one (Fig. 8 c).

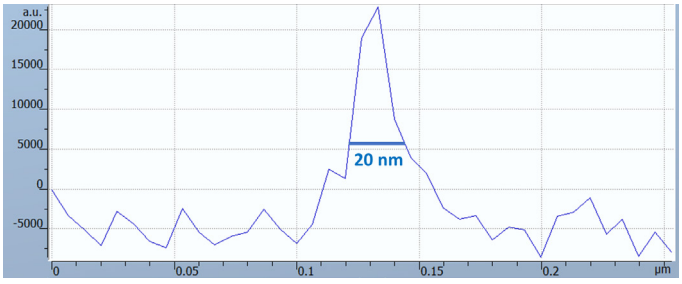

Figure 9: Section analysis of the TERS signal in water (2D band of the CNT) showing a 20 nm TER resolution.

In addition, the Full Width at Half Maximum (FWHM) of the TER intensity profile along the line across the CNT clearly demonstrates 20 nm spatial resolution (Fig. 9).

In our experiment, using a side backscattering configuration, this enhancement factor EF factor is given by [19]:

$$EF = \left(\frac{I_{nf}+I_{ff}}{I_{ff}}\right)\left(\frac{R_{focus}}{\frac{1}{2}R_{tip}}\right)^2 \cos\alpha$$

With R_{focus} = 1,200 nm (focal radius), R_{tip} = 20 nm (radius of curvature of the tip) and α = 60° (angle of incidence). I_{nf} and I_{ff} respectively stand for the component of the signal coming from the near-field (NF) and for the component of the signal coming from the far-field (FF).
Using this equation, the EF factor on the CNT calculated for the D band is

$$EF_{CNT} = 2.1\ x\ 10^5$$

Where I_{nf+Iff} = 14500 and I_{ff} = 1000.

Conclusion

AFM-TERS in liquids using side backscattering illumination has been demonstrated on GO and CNTs immersed in water. Specifics of the AFM-Raman setup that enable TERS in liquids have been presented: new side access liquid cell, integrated compensative optics, 25° inclined motorized approach, durable and accurate Raman laser-to-tip alignment with objective scanner. Thanks to those latest instrumental developments, we presented the nanoscale hyperspectral imaging of isolated carbon nanotubes in a liquid with a spatial optical resolution routinely obtained in TERS maps of 20 nm and stability for long term mapping. This work is expected to significantly broaden the potential applications of AFM-TERS wherein non-destructive and label-free chemical mapping in liquid environments presents a key measurement challenge.

Acknowledgements:

We thank Jana Kalbacova and Agnès Tempez for the manuscript correction. We thank Thomas Carlier for help in data processing.

References:

1. Tempez, A., Lancry, O., Krayev, A. & Chaigneau, M. Correlated TERS, TEPL and SPM Measurements of 2D Materials. https://www.horiba.com/en_en/tersfor2d/
2. Schmid, T., Yeo, B.-S., Leong, G., Stadler, J. & Zenobi, R. Performing tip-enhanced Raman spectroscopy in liquids. J. Raman Spectrosc. 40, 1392–1399 (2009).
3. Nakata, A., Nomoto, T., Toyota, T. & Fujinami, M. Tip-enhanced Raman Spectroscopy of Lipid Bilayers in Water with an Alumina- and Silver-coated Tungsten Tip. Anal. Sci. 29, 865–869 (2013).
4. Kumar, N., Wondergem, C. S., Wain, A. J. & Weckhuysen, B. M. In Situ Nanoscale Investigation of Catalytic Reactions in the Liquid Phase Using Zirconia-Protected Tip-Enhanced Raman Spectroscopy Probes. J. Phys. Chem. Lett. 10, 1669–1675 (2019).
5. Kumar, N. et al. Nanoscale chemical imaging of solid–liquid interfaces using tip-enhanced Raman spectroscopy. Nanoscale 10, 1815–1824 (2018).
6. Bhattarai, A. & El-Khoury, P. Z. Nanoscale Chemical Reaction Imaging at the Solid–Liquid Interface via TERS. J. Phys. Chem. Lett. 10, 2817–2822 (2019).
7. Bhattarai, A.; Joly, A. G.; Krayev, A.; El-Khoury, P. Z. Taking the Plunge: Nanoscale Chemical Imaging of Functionalized Gold Triangles in H2O via TERS. J. Phys. Chem. C 123 (12), 7376–7380 (2019).
8. Touzalin, T., Joiret, S., Maisonhaute, E. & Lucas, I. T. Complex Electron Transfer Pathway at a Microelectrode Captured by in Situ Nanospectroscopy. Anal. Chem. 89, 8974–8980 (2017).
9. Touzalin, T., Joiret, S., Maisonhaute, E. & Lucas, I. T. Capturing electrochemical transformations by tip-enhanced Raman spectroscopy. Curr. Opin. Electrochem. 6, 46–52 (2017).
10. Touzalin, T., Joiret, S., Lucas, I. T. & Maisonhaute, E. Electrochemical tip-enhanced Raman spectroscopy imaging with 8 nm lateral resolution. Electrochem. Commun. 108, 106557 (2019).
11. Chen, X., Goubert, G., Jiang, S. & Van Duyne, R. P. Electrochemical STM Tip-Enhanced Raman Spectroscopy Study of Electron Transfer Reactions of Covalently Tethered Chromophores on Au(111). J. Phys. Chem. C 122, 11586–11590 (2018).
12. Zeng, Z.-C.; Huang, S.-C.; Wu, D.-Y.; Meng, L.-Y.; Li, M.-H.; Huang, T.-X.; Zhong, J.-H.; Wang, X.; Yang, Z.-L.; Ren, B. Electrochemical Tip-Enhanced Raman Spectroscopy. J. Am. Chem. Soc. 137 (37), 11928–11931 (2015).
13. Huang, S.-C. et al. Electrochemical Tip-Enhanced Raman Spectroscopy with Improved Sensitivity Enabled by a Water Immersion Objective. Anal. Chem. 91, 11092–11097 (2019).
14. Martín Sabanés, N., Driessen, L. M. A. & Domke, K. F. Versatile Side-Illumination Geometry for Tip-Enhanced Raman Spectroscopy at Solid/Liquid Interfaces. Anal. Chem. 88, 7108–7114 (2016).
15. Sergey A. Saunin, Andrey V. Krayev, Vladimir V. Zhishimontov, Vasily V. Gavrilyuk, Leonid N. Grigorov, Alexey V. Belyaev, Dmitry A. Evplov, U.S. Patent US9910066, 2018
16. Su, W.; Kumar, N.; Krayev, A.; Chaigneau, M. In Situ Topographical Chemical and Electrical Imaging of Carboxyl Graphene Oxide at the Nanoscale. Nat. Commun. 9 (1), 2891 (2018).
17. Dresselhaus, M. S.; Jorio, A.; Hofmann, M.; Dresselhaus, G.; Saito, R. Perspectives on Carbon Nanotubes and Graphene Raman Spectroscopy. Nano Lett. 10 (3), 751–758 (2010).
18. Bhattarai, A.; Krayev, A.; Temiryazev, A.; Evplov, D.; Crampton, K. T.; Hess, W. P.; El-Khoury, P. Z. Tip-Enhanced Raman Scattering from Nanopatterned Graphene and Graphene Oxide. Nano Lett. 18 (6), 4029–4033 (2018).
19. HORIBA AFM-Raman FAQ: https://www.horiba.com/en_en/technology/measurement-and-control-techniques/microscopy-and-imaging/nanoraman/what-is-the-definition-of-ters-enhancement-factor/

HORIBA Scientific

info.sci@horiba.com

www.horiba.com/scientific

USA: +1 732 494 8660
UK: +44 (0)1604 542 500
China: +86 (0)21 6289 6060
Taiwan: +886 3 5600606
France: +33 (0)1 69 74 72 00
Italy: +39 06 51 59 22 1
India: +91 (80) 4127 3637
Brazil: +55 (0)11 2923 5400
Germany: +49 (0) 6251 8475 0
Japan: +81(75)313-8121
Singapore: +65 (6) 745-8300
Other: +33 (0)1 69 74 72 00